



## ICS ASSIGNMENT 1

# A Study on SIR Models and Extensions

\*\*\*\*\*

October 1, 2024

*Tutor:*  
Rafiazka Hilman

*Group:*  
C

*Student:*  
Ernani Hazbolatow  
14272210

*Lecturer:*  
Michael Lees  
*Course:*  
Introduction to Computational  
Science

*Course code:*  
5284ITCS6Y

## Contents

<b>1</b>	<b>Introduction</b>	<b>2</b>
<b>2</b>	<b>Background Information</b>	<b>3</b>
2.1	The <i>SIR</i> model . . . . .	3
2.2	The <i>SIR</i> model with Demography . . . . .	4
2.2.1	Eigenvalue Analysis of Equilibrium . . . . .	5
2.2.2	The Equilibrium of an Endemic Agent . . . . .	5
2.3	Infection-Induced Mortality for <i>SIR</i> with Demography . . . . .	6
2.4	Extensions of <i>SIR</i> : <i>SEIR</i> and <i>SEIRS</i> . . . . .	6
2.4.1	The <i>SEIR</i> model . . . . .	6
2.4.2	The <i>SEIRS</i> model . . . . .	7
2.4.3	Seasonal Forcing . . . . .	7
<b>3</b>	<b>Method</b>	<b>9</b>
3.1	Implementation of <i>SIR</i> models in Python . . . . .	9
3.2	Fitting <i>SIR</i> models in Python . . . . .	9
<b>4</b>	<b>Experiments</b>	<b>11</b>
<b>5</b>	<b>Results &amp; Discussion</b>	<b>13</b>

## 1 Introduction

Emerging wherever susceptible hosts gather, infectious diseases are a consistent companion to human civilization, often so with far ranging consequences. One such example is *Yersinia pestis*, the infectious agent behind the second plague pandemic in Europe. Although estimates vary, the rapid spread of the infectious agent is reckoned to have halved the human population in Europe [1].

We may ponder what could have happened to the spread of *Yersinia Pestis* under different conditions, such as varying levels of immunity, infectivity or changes in climate. For example, according to Schmid, Büntgen, Easterday, *et al.* [2], humid climates are conducive to the spread of *Yersinia Pestis*. Thus, it is likely that variations in these conditions could have altered the trajectory of the pandemic. With advances in modelling, these "what-if" questions can be studied. These models, in turn, may deliver insights which can guide policymakers in their decision-making during epidemics.

Therefore, this report investigates a range of compartment models within epidemiology to gain a better understanding of the behavior of epidemics through a series of experiments. First, we provide background information on the various compartment models used throughout this report. Initially, we present the basic *SIR* model and important concepts related to compartment models in epidemiology before extending the *SIR* model with demographic processes, infection-induced mortality and more compartments. Finally, we present a series of experiments integral to our understanding of infectious diseases and discuss their results.

---

## 2 Background Information

This section provides background information on the various compartment models in epidemiology used throughout this report. Initially, we present the basic *SIR* model. Second, we discuss how incorporating demographic processes into the basic *SIR* model can lead to persistent infectious agents. In addition, we introduce infection-induced mortality to the *SIR* model with demographics, no longer assuming a constant population. Lastly, we introduce two extensions of the *SIR* model, *SEIR* and *SEIRS*, using *Viral Rhinitis* as an example. Here, we also present seasonal forcing, specifically for the aforementioned extensions.

### 2.1 The *SIR* model

The *SIR* model, originally introduced by Kermack and McKendrick [3] to model how epidemics occur in closed populations, describes the movement of hosts through three compartments:

- **Susceptible:** Hosts who have not been previously exposed to the disease are susceptible. For the basic *SIR* model, no prior immunity exists in the population. Thus, all hosts are initially susceptible.
- **Infected:** Upon contact with infected individuals, susceptible hosts contract the disease and become infectious, contributing to the spread of the infectious agent within the population.
- **Recovered:** After a certain period, infectious hosts recover and acquire immunity, preventing reinfection.

According to Keeling and Rohani [4], the rate at which hosts move from compartment to compartment is determined by the following set of ordinary differential equations

$$\frac{dS}{dt} = -\beta SI \quad (1)$$

$$\frac{dI}{dt} = \beta SI - \gamma I \quad (2)$$

$$\frac{dR}{dt} = \gamma I \quad (3)$$

where  $S$ ,  $I$ , and  $R$  represent the proportions of the population in each compartment. The total population is constant throughout, implying  $S + I + R = 1$  at all times. Finally, there exists no prior immunity among the hosts in the population. The rate at which individuals move through compartments is determined by  $\beta$ , the transmission rate, and  $\gamma$ , the inverse of the recovery period (in days).

---

---

To understand why some infectious agents have the capacity to cause an epidemic, we introduce the basic reproductive number,  $R_0$ . As introduced by Keeling and Rohani [4],  $R_0$  represents "the average number of secondary infections by a single infected individual in a fully susceptible population". For the basic *SIR* model,  $R_0$  is equal to the ratio of the transmission rate to the recovery rate, expressed as

$$R_0 = \frac{\beta}{\gamma} \quad (4)$$

As shown in Figure 1, a  $R_0$  greater than 1 implies that the infectious agent spreads at a rate greater than the recovery rate, leading to a growing number of infections over time. After some time, the number of infections peak and growth stops. The number of infected people start to decline as infectious hosts recover. Eventually, the infectious agent reaches extinction in the population.

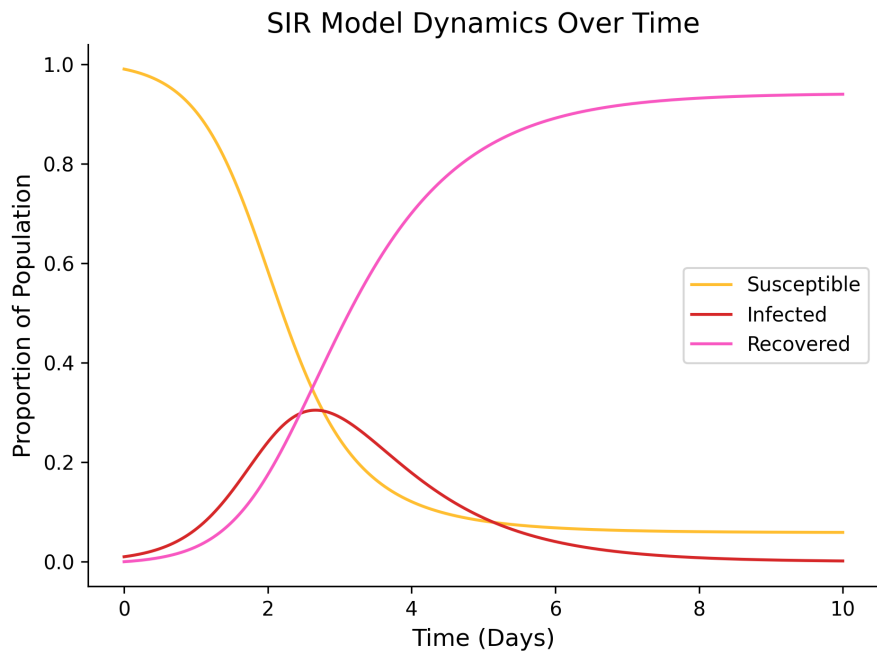


Figure 1: The Dynamics of an  $R_0 > 1$  Infectious Agent ( $\beta = 3, \gamma = 1$ ) Modelled by *SIR*

In contrast, when  $R_0$  is less than 1, the infection declines without intermediately peaking, with individuals recovering faster than new infections occurring.

## 2.2 The SIR model with Demography

One of the limitations of the basic *SIR* model is that it is unable to accurately represent persistent infectious diseases [4] [5]. For these diseases, demographic processes such as natural birth and death play a significant role in their long-term dynamics. To address this limitation, the *SIR* model with demographic processes expands upon the basic *SIR* model with a new parameter,  $\mu$ .  $\mu$  represents the natural birth and death rate in the population. According to Best [5], the system of ordinary differential equations changes to

$$\frac{dS}{dt} = \mu - \beta SI - \mu S \quad (5)$$

$$\frac{dI}{dt} = \beta SI - I(\gamma + \mu) \quad (6)$$

$$\frac{dR}{dt} = \gamma I - \mu R \quad (7)$$

where the population size remains constant, as births balance deaths over time. The inclusion of  $\mu$  alters the definition of  $R_0$ , now defined as

$$R_0 = \frac{\beta}{\gamma + \mu} \quad (8)$$

More importantly, the inclusion of  $\mu$  fundamentally alters the long-term dynamics of the basic *SIR* model. In the absence of demographic effects, the basic *SIR* model predicts that epidemics necessarily undergo extinction once a sufficient portion of the population has recovered, leaving behind too few susceptible individuals to sustain transmission [4]. However, with demographic processes in play, the increase of the susceptible population via births and the removal of the recovered population via deaths can allow the disease to persist indefinitely. This results in the possibility of an endemic equilibrium where the disease remains in the population at a steady level rather than going extinct [5].

### 2.2.1 Eigenvalue Analysis of Equilibrium

In order to understand how infectious agents either reach disease-free states or endemic states, we briefly dive into the mathematical framework that governs the dynamics behind the equilibria of dynamical systems. Per Strogatz [6], an equilibrium occurs "when the state variables no longer change". Therefore, for *SIR* models, equilibria occur when the system of ordinary differential equations satisfy the following equality

$$\frac{dI}{dt} = \frac{dS}{dt} = \frac{dR}{dt} = 0$$

which indicates that  $S$ ,  $I$  and  $R$  no longer change. Possible values for  $S$ ,  $I$  and  $R$  that satisfy the above equality are henceforth labelled as  $S^*$ ,  $I^*$  and  $R^*$ .

To understand if (and how) a dynamical system reaches an equilibrium, an Eigenvalue analysis of the Jacobian matrix,  $\mathbf{J}$ , of the dynamical system can be performed [6]. Eigenvalue analysis involves finding the eigenvalues,  $\vec{\lambda}$ , that satisfy the following equality

$$\det(\mathbf{J} - \vec{\lambda}\mathbf{I}_m) = 0 \quad (9)$$

where  $\mathbf{I}_m$  is the Identity matrix. According to Keeling and Rohani [4] and Best [5] the Jacobian of the *SIR* model with demographic processes is equal to

$$\mathbf{J} = \begin{pmatrix} -\beta I^* - \mu & -\beta S^* \\ \beta I^* & \beta S^* - (\gamma + \mu) \end{pmatrix} \quad (10)$$

Although there are three ordinary differential equations, we omit  $\frac{dR}{dt}$  by assuming a constant population. Therefore, we find the values for  $\lambda_{1,1}$  and  $\lambda_{2,2}$  that satisfy

$$\det \left( \begin{pmatrix} -\beta I^* - \mu - \lambda_{1,1} & -\beta S^* \\ \beta I^* & \beta S^* - (\gamma + \mu) - \lambda_{2,2} \end{pmatrix} \right) = 0 \quad (11)$$

### 2.2.2 The Equilibrium of an Endemic Agent

We shift our focus to persistent infectious agents. Keeling and Rohani [4] provides the endemic equilibrium point for *SIR* models with demographic processes as

$$(S^*, I^*, R^*) = \left( \frac{\gamma + \mu}{\beta}, \frac{\mu}{\beta}(R_0 - 1), 1 - S^* + I^* \right) \quad (12)$$

Because the population size is constant, we find  $R^*$  in terms of  $S^*$  and  $I^*$ . An approximate solution of  $\vec{\lambda}$  for endemic agents exists, equal to

$$\vec{\lambda} \approx -\frac{\mu R_0}{2} \pm \frac{1}{\sqrt{AC}} i \quad (13)$$

where  $i = \sqrt{-1}$ ,  $A = \frac{1}{\mu(R_0 - 1)}$  and  $G = \frac{1}{\mu + \gamma}$ .

When  $\lambda$  has both real and imaginary components, implying that the eigenvalues have the form  $\lambda = a \pm xi$ , we can classify if (and how) the system reaches the equilibrium by investigating the real scalar component,  $a$ . Because  $\mu$  is always positive and  $R_0$  cannot be negative,  $-\frac{\mu R_0}{2}$  is always negative. According to Strogatz [6], if the real part of the eigenvalue is negative, this implies that the equilibrium is stable and approached by a damped oscillator. According to Keeling and Rohani [4], the rate of dampening,  $D$ , is equal to the real part of the eigenvalue

$$D = -\frac{\mu R_0}{2} \quad (14)$$

Furthermore, the rate of oscillations,  $T$ , is equal to

$$T \sim 2\pi\sqrt{AG} \quad (15)$$

### 2.3 Infection-Induced Mortality for *SIR* with Demography

Until now, deaths were attributed solely to demographic processes. However, some infectious agents directly cause death. The probability of mortality due to the infectious agent,  $\rho$ , affects the ordinary differential equation for  $\frac{dI}{dt}$ , which becomes

$$\frac{dI}{dt} = \beta SI - I \left( \frac{\gamma + \mu}{1 - \rho} \right) \quad (16)$$

Prior, births balanced deaths over time. Now, if the rate of demographic processes still equal each other, the population no longer stays constant. Still, this system reaches an endemic state by damping oscillations if  $R_0 > 1$  [4].

### 2.4 Extensions of SIR: *SEIR* and *SEIRS*

Infection with *Viral Rhinitis*, also known as the common cold, involves a latency period where the host is infected but not infectious [7]. For *Viral Rhinitis*, this transitional period ranges in between 1 to 7 days [8]. The previously introduced *SIR* model and its variants assume no latency period. For these models, being infected implies being able to infect. Thus, they are unable to accurately model *Viral Rhinitis* and similar infectious agents. Therefore, we introduce two extensions of the *SIR* model, *SEIR* and *SEIRS*, which are better suited to model infectious agents like *Viral Rhinitis*.

#### 2.4.1 The *SEIR* model

In the *SEIR* (and *SEIRS*) model, these hosts reside in a new compartment, Exposed. Upon contact with infected individuals, susceptible hosts contract the disease. However, these hosts, although infected, do not contribute to the spread of the infectious agent yet [7]. The rate at which hosts move from the Exposed compartment to the Infected compartment is determined by the parameter  $\sigma$  [4]. Similarly to  $\gamma$ ,  $\sigma$  is defined as the inverse of the average latent period (in days). Thus, the system of ordinary differential equations for *SEIR* becomes

$$\frac{dS}{dt} = \mu - (\beta S + \mu)S \quad (17)$$

$$\frac{dE}{dt} = \beta SI - E(\sigma + \mu) \quad (18)$$

$$\frac{dI}{dt} = \sigma E - (\mu + \gamma)I \quad (19)$$

$$\frac{dR}{dt} = \gamma I - \mu R \quad (20)$$

The inclusion of a new compartment affects the definition of  $R_0$  [7]. For the *SEIR* model,  $R_0$  is equal to

$$R_0 = \left( \frac{\sigma}{\sigma + \mu} \right) \times \left( \frac{\beta}{\gamma + \mu} \right) \quad (21)$$

#### 2.4.2 The *SEIRS* model

For *Viral Rhinitis*, demographic processes are not solely responsible for new influxes of susceptible hosts. Eventually, recovered hosts lose their immunity over time and become susceptible again [9]. Bjørnstad, Shea, Krzywinski, *et al.* [7] extend *SEIR* model by introducing waning immunity, resulting in the *SEIRS* model. Recovered hosts lose their built-up immunity at a rate determined by  $\omega$ , which is the inverse of the average period (in days) that a recovered individual retains immunity. To visualize the flows between compartments, Figure 2 shows a schematic diagram of stock and flows for the *SEIRS* model.

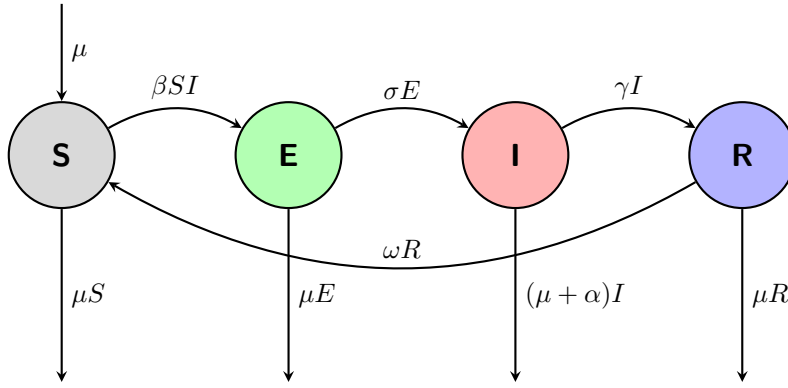


Figure 2: Stock and Flow Diagram of the *SEIRS* model, adapted from Bjørnstad, Shea, Krzywinski, *et al.* [7]

The system of ordinary differential equation for the *SEIRS* model is equal to

$$\frac{dS}{dt} = \mu S - \beta SI + \omega R \quad (22)$$

$$\frac{dE}{dt} = \beta SI - (\sigma + \mu)E \quad (23)$$

$$\frac{dI}{dt} = \sigma E - (\gamma + \mu)I \quad (24)$$

$$\frac{dR}{dt} = \gamma I - (\mu + \omega)R \quad (25)$$

$\omega$  does not alter the expression of  $R_0$  as given by Equation (21).

#### 2.4.3 Seasonal Forcing

In many populations, infections with *Viral Rhinitis* primarily occur when temperatures cool down during autumn and winter [8]. According to Lowen and Steel [10], this seasonal trend can be attributed to several factors:

- *Viral Rhinitis* is more stable at colder temperatures, allowing for increased transmission among hosts.
- Colder temperatures affect the host's nasal epithelia, lowering their innate defense against *Viral Rhinitis*

Therefore, in order to model *Viral Rhinitis* properly, the transmission term should no longer be constant and instead be temperature-dependent. For example,  $\beta(t)$  could take the form

$$\beta(t) = \beta_0(1 + K(t)) \quad (26)$$

---

where  $\beta_0$  is the average transmission rate and  $K(T)$  is a function used to model periodic phenomena such as  $\sin(x)$  or  $\cos(x)$ . For *Viral Rhinitis*, a possible form  $\beta(t)$  could take is

$$\beta(t) = \beta_0 + \beta_0 A_0 \left(1 - \frac{T(t)}{T_{\text{avg}}}\right) \quad (27)$$

$$T(t) = T_{\text{avg}} + T_{\text{avg}} \sin \left( 2\pi \left( \frac{t}{365} - 0.25 \right) \right) \quad (28)$$

where  $T_{\text{avg}}$  is the yearly average temperature and  $t$  is a day in a year. Here,  $A_0$  determines the effect of seasonal forcing. When  $A_0 = 0$ ,  $\beta(t)$  is equal to  $\beta_0$ . However, when  $A_0 > 0$ , the temperature influences the transmission rate. Figure 3 illustrates the effect of temperature on the transmission term when seasonal forcing is introduced. As temperature at time  $t$  exceeds the yearly average temperature,  $\beta(t)$  is less than  $\beta_0$ . When temperatures sink below the yearly average temperature,  $\beta(t)$  is greater than  $\beta_0$

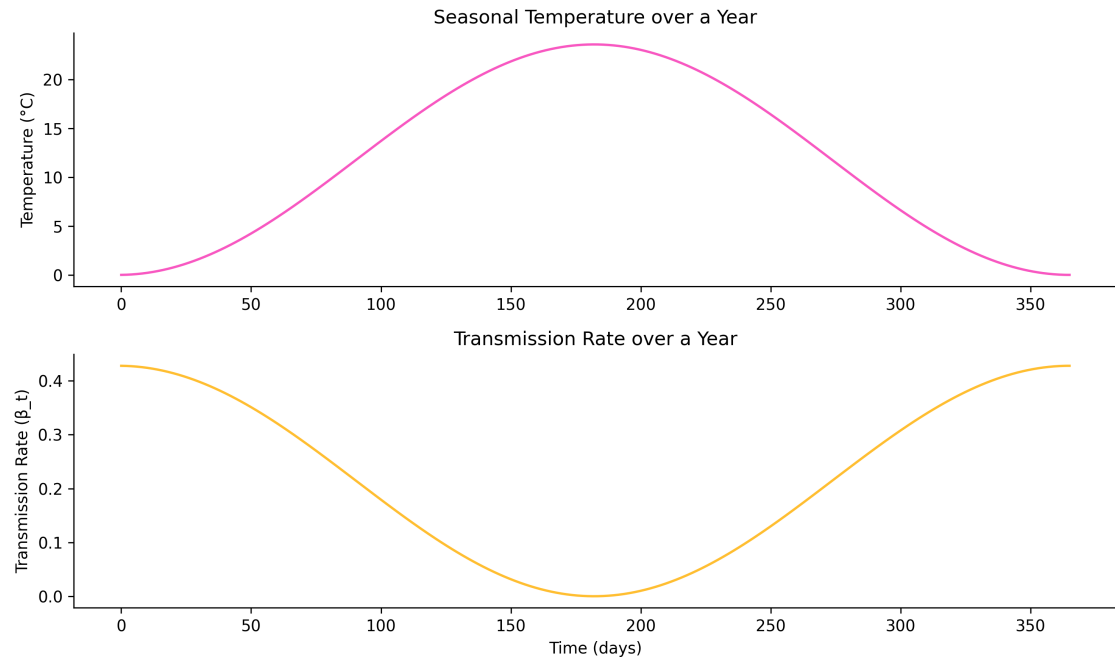


Figure 3: Impact of Temperature on Transmission Rate, retrieved from *SEIRS* model (with  $\beta_0 = 0.214$  and  $A_0 = 1$ )

### 3 Method

All experiments were programmed and executed using Python (version 3.12.4), utilizing a range of scientific libraries such as NumPy [11] for general array handling and manipulation, SciPy [12] for Fourier and Eigenvalue analyses, Matplotlib [13] for visualization and math for mathematical constants.

#### 3.1 Implementation of *SIR* models in Python

The `SIRbase` Python class implements the basic *SIR* model described in Section 2.1. This class consists of the following methods:

- `__init__(beta, gamma, I0)` initializes a basic *SIR* model using function parameters such as the infection rate  $\beta$ , recovery rate  $\gamma$ , and the initial infected proportion  $I_0$ . The initial states of the susceptible  $S$  and recovered  $R$  depend on  $I_0$ .
- A set of functions that individually return the values of the differential equations for the susceptible and infected populations, namely `dSdt(S, I)` and `dIdt(S, I)`.
- An `update_step(dt = 0.01)` function that uses the Runge-Kutta 4th-order (RK4) method to update the state of the model over a single time step. The implementation of KR4 closely follows the procedure described by Press, Teukolsky, Vetterling, *et al.* [14]. This method applies RK4 to both `dSdt` and `dIdt` and updates values for  $S$  and  $I$ . The default step size is equal to 0.01. However, for some experiments, the step size was lowered in order to prevent spurious dynamics [4].
- An `numerical_integration(t, dt = 0.01)` function that applies `update_step(dt = 0.01)` for  $t \times dt$  time steps. This function iterates over  $t$  days and returns arrays of  $t$ ,  $S$ ,  $I$  and  $R$  values.

This class serves as the foundation for further extensions through inheritance, allowing for additional features to be integrated into the model, such as vaccination protocols or demographic processes. Although the `SEIRS` model described in Section 2.4 does not directly inherit from `SIRbase`, `SEIRS` follows the design principles set out above.

#### 3.2 Fitting *SIR* models in Python

The `SIRsolver` class optimizes the parameters of an *SIR* model by minimizing the loss function through gradient-based optimization. `SIRsolver` implements the following methods:

- `computeLoss(params, obsS)`: This function computes the value of the loss function by running the *SIR* model for set of model parameters. Although any continuous loss function can be passed as the loss function in `SIRsolver`, the only implemented loss function is the mean squared error. `MSE(estimated_data, observed_data)` computes the mean squared error between the observed data and the estimated data generated by the model, equal to [15]

$$\text{MSE} = \frac{1}{n} \sum_{i=1}^n (y_i - \hat{y}_i)^2$$

- `computeGrad(obsS, params, epsilon=1e-8)`: This function calculates the gradient of the loss function with respect to the model parameters using finite differences. The finite difference scheme follows the implementation by Press, Teukolsky, Vetterling, *et al.* [14]. The default step is set to 1e-8.
- `optimize(obsS, learning_rate=0.01, max_iterations=1000, epsilon=1e-8)`: This function performs gradient-based optimization using the AdaGrad algorithm (see pseudo-code below). Like other gradient-based optimization algorithms, AdaGrad iteratively adjusts the model parameters to minimize the loss by computing the gradient and updating

the parameters accordingly (until the loss is minimized or a maximum number of iterations is reached). In addition, AdaGrad allows for larger updates to some model parameters depending on the size of the gradient, which can lead to a quicker convergence to a local or global minima [15]. The optimization process outputs the best-fitting model parameters, along with the lowest loss achieved during the iterations.

**AdaGrad Pseudocode [15]**

```
Initialize: learning rate  $\eta, \epsilon = 10^{-8}$ , initial weights  $\theta_0$ , gradient sum  $G = 0$ , max iterations  $T = 1000$ 
for each iteration  $t = 1, 2, \dots, T$  do
    1. Compute gradient:  $g_t = \nabla_{\theta} J(\theta_t)$ 
    2. Accumulate squared gradients:  $G = G + g_t^2$ 
    3. Update weights:  $\theta_{t+1} = \theta_t - \frac{\eta}{\sqrt{G+\epsilon}} \cdot g_t$ 
end for
```

The *solverSIR* class works for any SIR model that follows the same structure as **SIRbase**.

## 4 Experiments

We conducted a series of experiments in order to explore various aspects of infectious disease dynamics. Firstly, to investigate which parameter determines if an infectious disease will cause an epidemic, we created a series of phase diagrams for *SIR* models with different values for  $\beta$  and  $\gamma$ . The discussion on  $R_0$  presented in Section 2.1 guided the selection of the parameter values, where a pair of parameter values were either labelled as extinctive ( $R_0 < 1$ ) or epidemic ( $R_0 > 1$ ). The chosen pairs are provided in Table 1.

Categorization	$(\beta, \gamma)$
Extinctive ( $R_0 < 1$ )	(0.5, 2), (1.83, 2.00)
Epidemic ( $R_0 > 1$ )	(2.00, 1.83), (2.00, 0.50)

Table 1: Extinction vs Epidemic Parameter Values

Secondly, to investigate the validity of the basic *SIR* model for acute infections in closed populations, we fit a basic *SIR* model to data of an influenza outbreak. Table 2 contains the parameters used for the fitting procedure.

Parameter	Value
Initial State ( $\beta, \gamma$ )	(1, 1)
Maximum Iterations	1000
Learning rate	0.025
Finite Differences Step Size	$1 \times 10^{-8}$

Table 2: Settings for Fitting Procedure

Then, we devised two vaccination protocols for this specific outbreak. These vaccination protocols are briefly described below:

1. **Zero-Day Vaccination:** Susceptible hosts are vaccinated at a flat vaccination rate,  $\alpha$ , from the onset of the epidemic. Therefore, the differential equations for the susceptible and recovered population now include the removal of susceptible hosts by vaccination, such that

$$\frac{dS}{dt} = -\beta SI - \alpha S \quad (29)$$

$$\frac{dR}{dt} = \gamma I + \alpha S \quad (30)$$

2. **Dynamic Vaccination:** The number of susceptible hosts are vaccinated based on a dynamic vaccination rate. The dynamic vaccination rate is controlled by a logistic function that increases as infections approach the maximum capacity of infected individuals,  $\theta$ , a population can handle. Like  $I$ ,  $\theta$  is expressed as a proportion. The dynamic vaccination rate function is equal to

$$\frac{\alpha_{\max}}{1 + e^{-5(I-\theta)}} \quad (31)$$

Thus, the differential equations change to

$$\frac{dS}{dt} = -\beta SI - \frac{\alpha_{\max}}{1 + e^{-5(I-\theta)}} S \quad (32)$$

$$\frac{dR}{dt} = \gamma I + \frac{\alpha_{\max}}{1 + e^{-5(I-\theta)}} S \quad (33)$$

We used  $\alpha$  values ranging from 0 to 0.1 to assess the Zero-Day vaccination protocol's effectiveness. Furthermore, we assessed the Dynamic Vaccination protocol's effectiveness for  $\alpha_{\max} \in [0, 0.2]$  and  $\theta \in [0.05, 0.3]$ . In both cases, we measured the effectiveness of the vaccination protocol by observing the decrease in peak infections.

Next, to investigate persistent infectious agents, we analyzed a hypothetical persistent infectious agent using a *SIR* model with demographic processes. Based on the Eigenvalue analysis presented in Section 2.3, the values for  $\beta$ ,  $\gamma$ , and  $\mu$  were chosen to ensure that long-term dynamics could be observed. These values are given in the Table 3.

Parameter	Value
$\beta$ (Transmission rate)	1
$\gamma$ (Recovery rate)	$\frac{3}{10}$
$\mu$ (Birth/Death rate)	$\frac{1}{20}$
$t$ (Model time)	200 days
$dt$ (Step size RK4)	0.005

Table 3: Parameter Values for a Persistent Infectious Agent

Furthermore, we created phase diagrams to visualize the long-run behavior of this persistent infectious agent. In order to verify the results of the Eigenvalue analysis, we conducted a Fourier analysis and computed the decay rate and oscillation period. Finally, we added infection-induced mortality to the *SIR* model with demographic processes. In order to understand how infection-induced mortality affects the endemic status of this persistent infectious agent, we ran several *SIR* models for different values of  $\rho$ , using the same parameter values mentioned in Table 3.

Finally, we used a *SEIRS* model to investigate the long-run dynamics of persistent infectious agents with waning immunity. Here, we verified the *SEIRS* model using the parameters from Bjørnstad, Shea, Krzywinski, *et al.* [7], provided in Table 4. According to Keeling and Rohani [4], the latency period has no effect on an infectious agent's long-term dynamics. Therefore, we restricted ourselves to observing how dynamics of persistent infectious change by examining various values of the waning immunity. The values chosen are equal to  $\frac{1}{\omega} = \frac{1}{182.5}$ ,  $\frac{1}{365}$  and  $\frac{1}{730}$ . To properly capture the effect of slow waning immunity, the model ran for 10 years. Then, we added seasonal forcing to the *SEIRS* model, modelling  $\beta(t)$  using Equation 27. We investigated the effects of seasonal forcing by performing and plotting the *SEIRS* models and Fourier analyses for different levels of seasonal forcing, again for 10 years.

Parameter	Value
$\beta$ (Transmission rate)	0.214
$\gamma$ (Recovery rate)	$\frac{1}{14}$
$\sigma$ (Incubation rate)	$\frac{1}{7}$
$\mu$ (Birth/Death rate)	$\frac{1}{76 \times 365}$
$I_0$ (Initial infected population)	0
$E_0$ (Initial exposed population)	0.001
$\omega$ (Waning immunity rate)	$\frac{1}{365}$
$t$ (Model Time)	1825 Days

Table 4: Parameter Values for SEIRS Model from Bjørnstad, Shea, Krzywinski, *et al.* [7]

## 5 Results & Discussion

To investigate which parameter determines if an infectious agent in a closed population can develop into an epidemic, we investigate four phase diagrams. Using Figure 4, we show that when  $R_0$  is less than 1, an epidemic is impossible. Across all initial values for the infected proportion, the proportion of infected individuals in the population flow to 0 without an intermediate peak. When  $R_0$  is greater than 1, an epidemic is possible, although dependent on the initial value of

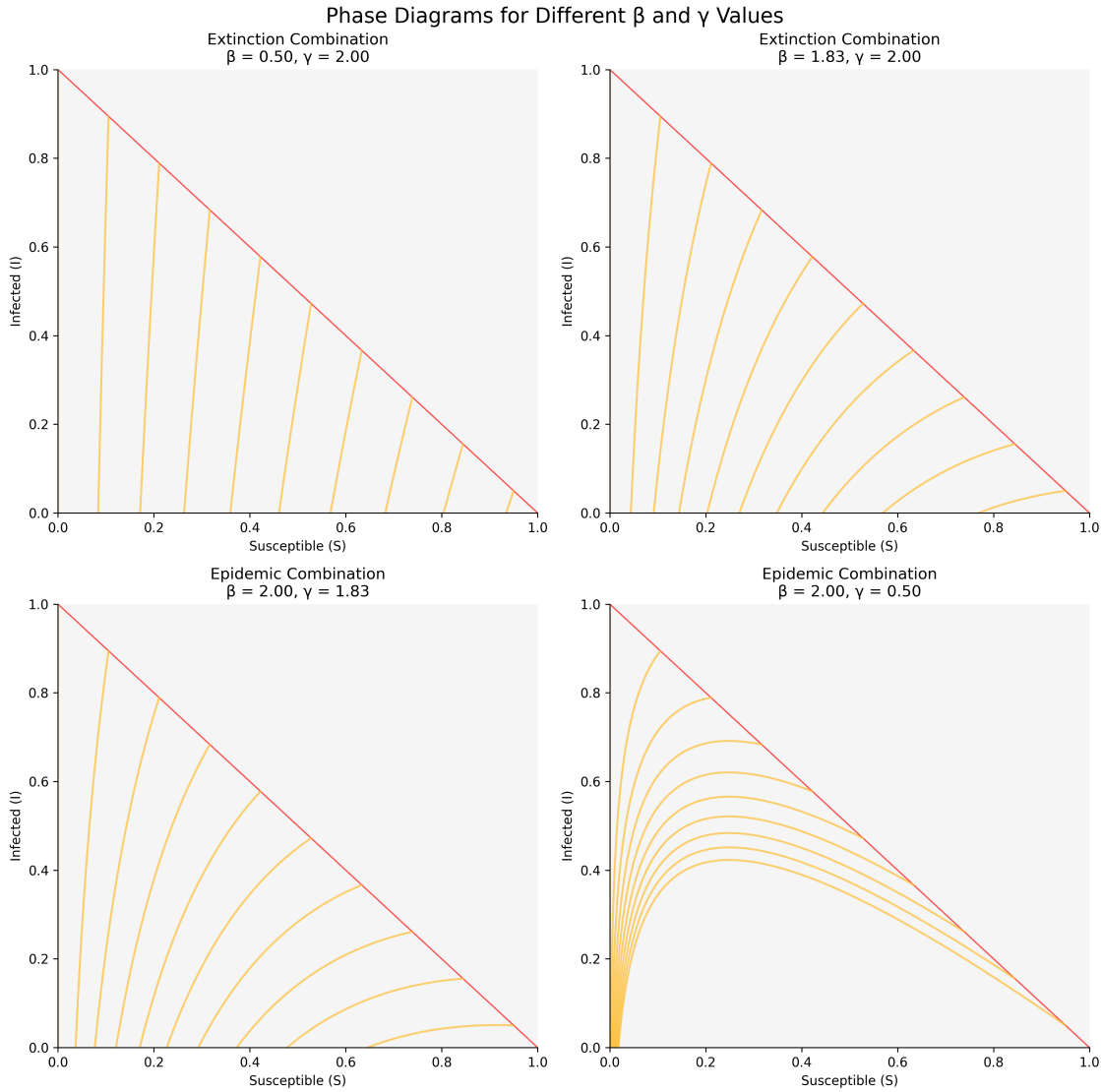


Figure 4: Phase Plots for Different Combinations of  $\beta$  and  $\gamma$

I. For example, the infectious agent with  $\beta = 2$  and  $\gamma = 1.83$  only peaks when the initial value of  $I$  is small enough. This can be explained by the ordinary differential equation for the infected population,  $\frac{dI}{dT}$ . When setting Equation (2) to 0 and  $I = I_0$ , we observe

$$\begin{aligned} 0 &= 2SI - 1.83I \\ &= I_0(2(1 - I_0) - 1.83) \end{aligned}$$

which implies that the number of infections only increases when the initial proportion of infections is less than 0.085. For this infectious agent, choosing a starting value for  $I_0$  greater than 0.085 implies that the infectious agent has already peaked and is undergoing extinction.

---

To investigate the validity of the basic *SIR* model for acute infections in closed populations, we fit a basic *SIR* model to data of an influenza outbreak. With a mean squared error loss of approximately 0.0004, the best fitting values for  $\beta$  and  $\gamma$  are approximately equal to 1.6655 and 0.4523 respectively. As seen in Figure 5, the basic *SIR* model fits to the data well. Therefore, the basic *SIR* adequately models acute infections in closed populations.

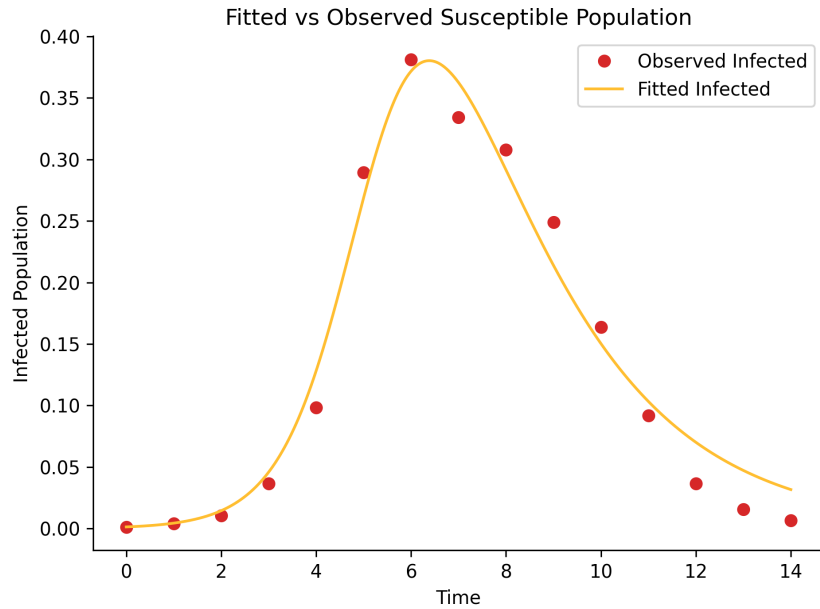


Figure 5: Model Fit for School Influenza Data,  $\beta \approx 1.665$ ,  $\gamma \approx 0.452$

For the Influenza outbreak, we explored two vaccination protocols that could limit the epidemic observed and evaluate their effectiveness. The results of both protocols are shown in Figure 6. First, we consider a Zero-Day vaccination program with a flat vaccination rate. Figure 6a shows the effectiveness of a Zero-Day vaccination program at reducing the peak number of infections. We observe the greatest reduction for the highest flat vaccination rate, reducing the peak number of infections from 290 to 85. Although this vaccination protocol is effective, the practical limitations are apparent. First, a vaccination program cannot start from day 0. The introduction of an infectious agent needs to be detected before pupils can be inoculated against the agent. In addition, even if the infectious agent were to be detected as early as day 0, the logistical efforts behind a vaccination protocol would limit a large number of vaccinations from the get-go. Therefore, although theoretically effective, a Zero-Day vaccination protocol with a flat vaccination rate has practical limitations.

Second, we consider a vaccination program with a dynamic vaccination rate. Figure 6b illustrates how, as the maximum vaccination rate rises and the maximum capacity falls, the peak of infections is significantly reduced. In our results, the maximum capacity and the maximum vaccination rate have a non-linear relationship. At low values for the maximum vaccination rate, maximum capacity is non-influential to the decrease in the peak infected. However, maximum capacity becomes more important for reducing peak infections as the maximum vaccination rate increases. Like Zero-Day vaccination, Dynamic intervention assumes vaccination from day 0 is possible. However, only  $\frac{1}{763}$  of the population is infected at day 0. Therefore, the effective vaccination rate at day 0 is close to 0. Dynamic intervention has the advantage of allowing for a gradual increase in vaccinations over time. Vaccinations, as the epidemic progresses, increase over time.

\*\*\*\*\*

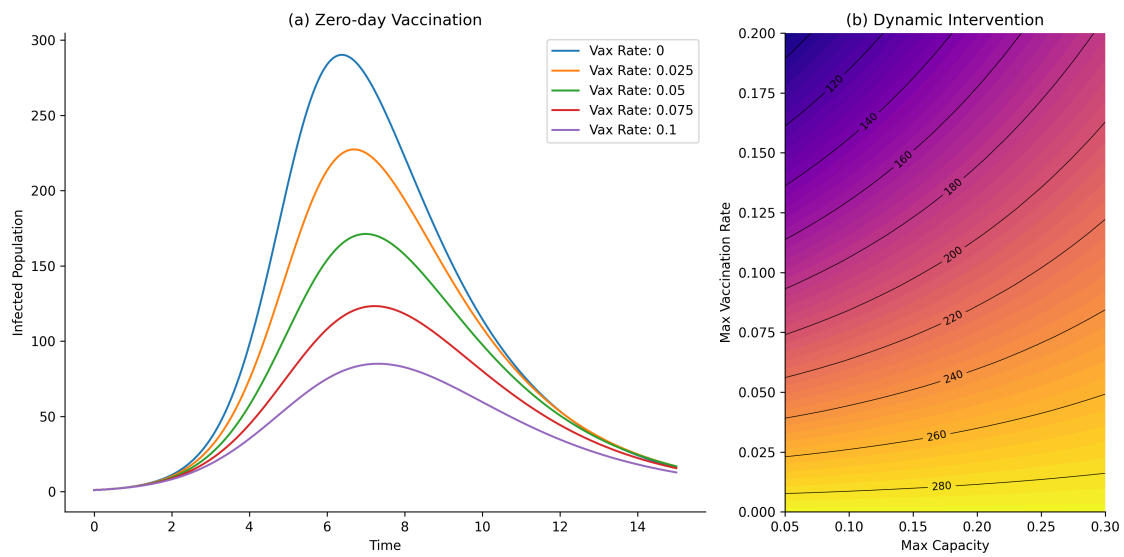


Figure 6: Impact of Vaccination Protocols on Total Peak Infected.

To understand how infectious diseases persist in a population, we modelled a hypothetical infectious agent using a *SIR* model with demographic processes. For this infectious agent, an Eigenvalue analysis was performed. As shown in the Eigenvalue analysis below, the infectious agent reaches an endemic status. The endemic equilibrium is equal to  $S^* \approx 0.35$  and  $I^* \approx 0.093$ .

```
eigenvalue_analysis(beta = 1, gamma = 0.3, mu = 1/20)
# Eigenvalues of the Jacobian: [-0.07142857+0.16552329j -0.07142857-0.16552329j]
# The endemic equilibrium is stable and approaches the endemic equilibrium:
# (S: 0.35, I: 0.09285714285714286)
# The system has an oscillation period of 0.0287 and decay rate of -0.0714.
```

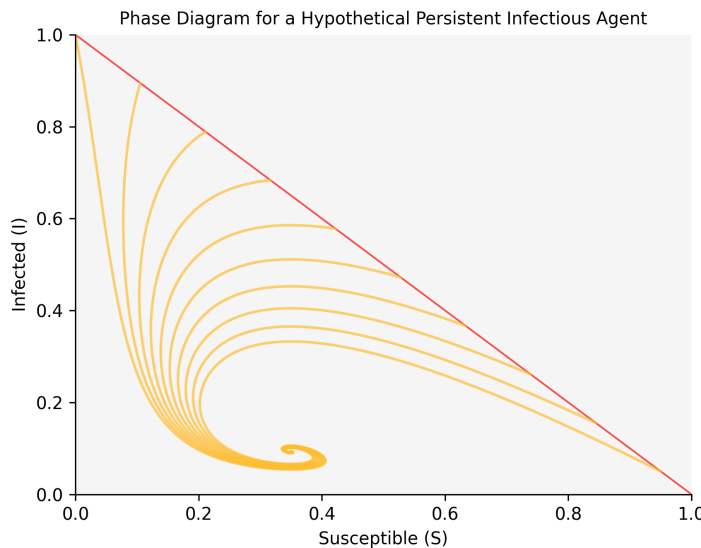


Figure 7: Phase Diagram of the Hypothetical Persistent Infectious Agent

\*\*\*\*\*

---

To visualize this equilibrium, we created a phase diagram. As seen in Figure 7, we observe that for all initial values of  $I$ , the hypothetical persistent infectious agent flows to the endemic equilibrium point found in the Eigenvalue analysis. Furthermore, the Fourier analysis provides more information about the oscillation period of this infectious agent. In our results, shown in Figure 8, there is a clear peak at approximately 0.0287. This implies that the oscillation take  $\frac{1}{0.0287} \approx 35$  days. The oscillations are damped over time, ensuring that an endemic equilibrium is reached, as shown in Figure 7.

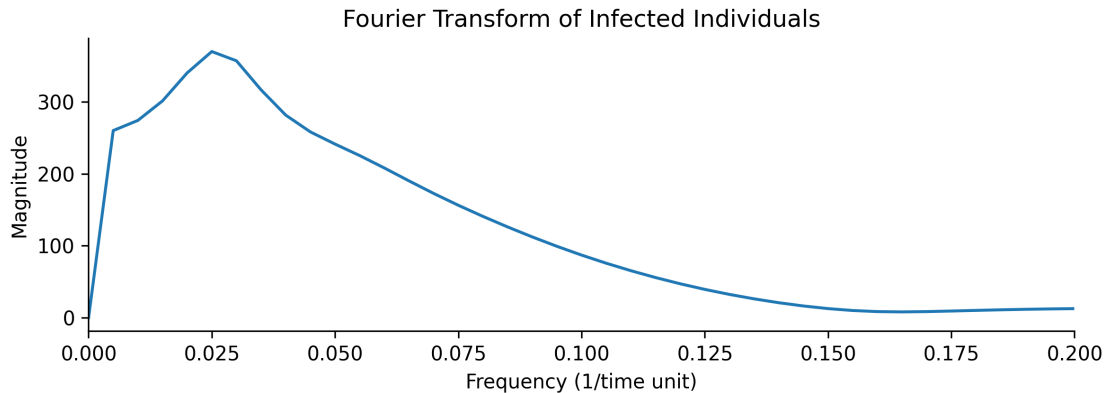


Figure 8: Result of the Fourier Analysis

To understand how the inclusion of infection-induced mortality affects whether an infectious agent reaches an endemic state or undergoes extinction, we analyzed the same hypothetical infectious agent for different values of  $\rho$ . Previously, the infectious agent reached an endemic state of  $S^* \approx 0.35$  and  $I^* \approx 0.093$ . Now, as shown in Figure 9, as  $\rho$  increases,  $I^*$  decreases linearly. At  $\rho \approx 0.65$ ,  $I^*$  is equal to 0. Beyond 0.65, the infectious agent is no longer endemic and undergoes extinction. Therefore, high infection-induced mortality is not conducive to endemic states, as infectious agents cannot spread via deceased hosts.

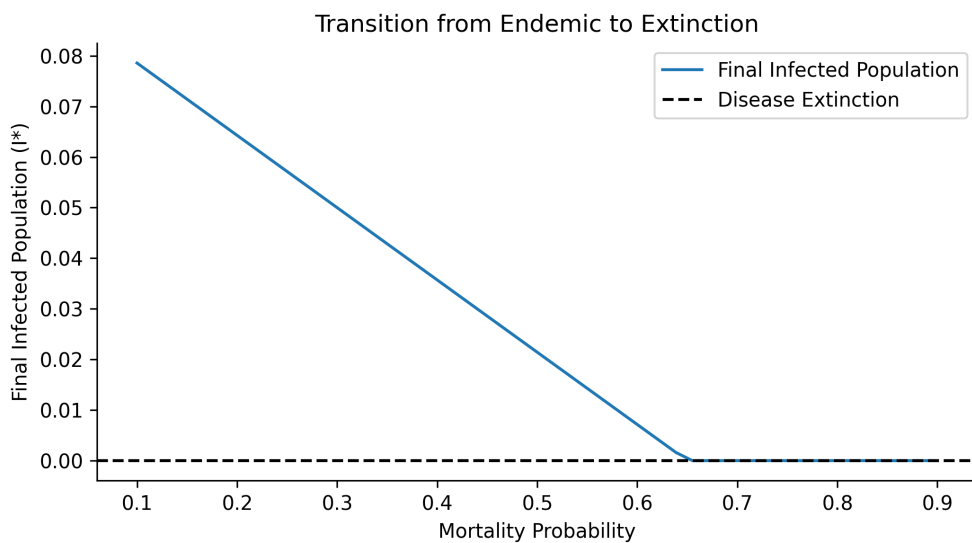


Figure 9: Impact of Infected-Induced Mortality on the Value of  $I^*$

---

The *SEIRS* model expands upon the *SIR* model with a latency period and waning immunity. Previously, we investigated the long-term dynamics of infectious agents modelled with the *SIR* model. Now, we turn to infectious agents modelled with *SEIRS*. We plot phase planes for different values of  $\omega$ . Figure 10 shows that endemic equilibria exist for all values of  $\omega$ . Thus, the infectious agent retains its endemic status. However, based on our results, we observe that a longer waning immunity correlates with a lower proportion of infected individuals at equilibrium. When immunity wanes more slowly, the rate of new infections is reduced. This, in turn, causes lower levels of  $I^*$ . Therefore,  $\omega$  influences the intensity of endemic infections rather than the agent's ability to remain endemic.

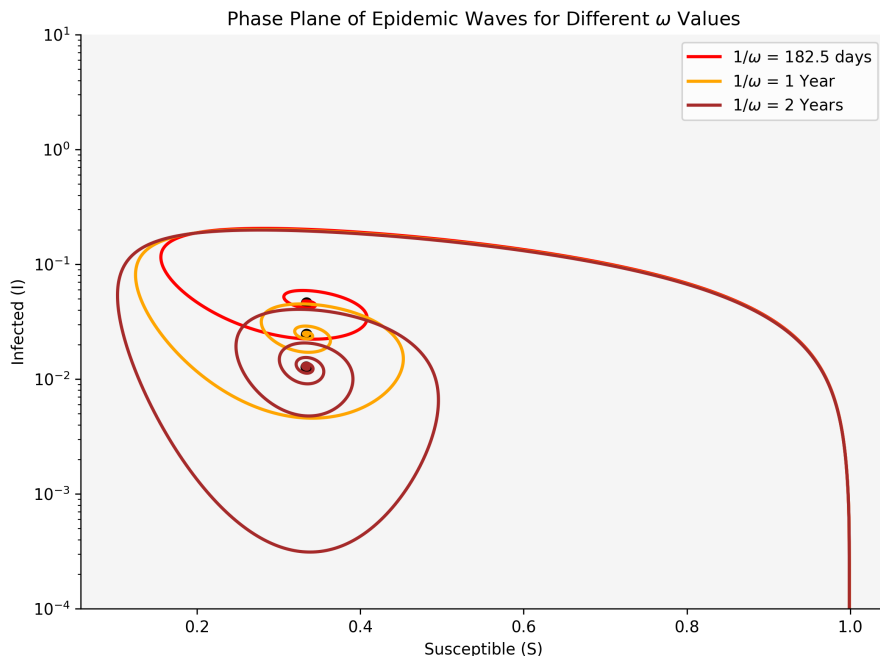


Figure 10: Long-Term Dynamics of *SEIRS* with Different Values for  $\omega$

Finally, we investigated the effect of seasonal forcing on the *SEIRS* model on the long-term dynamics of an infectious agent. As shown in Figure 11, the long-term dynamics differ when seasonal forcing is applied. Without seasonal forcing, the infectious agent reaches a steady endemic equilibrium. The accompanying Fourier analyses shows a singular dominant peak, indicating stable, long-term dynamics. For  $A_0 = 0$ , the oscillating period is equal to  $\frac{1}{0.002465} = 405.56$  days. When  $A_0 = 0.3$ , the infectious agent no longer reaches an endemic equilibrium. From our results, we observe recurring epidemics every year. The Fourier analysis captures this behavior by showing dominant peaks at multiples of 0.00274. When  $A_0 = 0.5$ , we observe the same behavior as  $A_0 = 0.3$ , but to a greater extent. Thus, the introduction of seasonal forcing destabilizes the endemic equilibrium and leads to recurring epidemics. As seasonal forcing increases, so does the complexity of the epidemics.

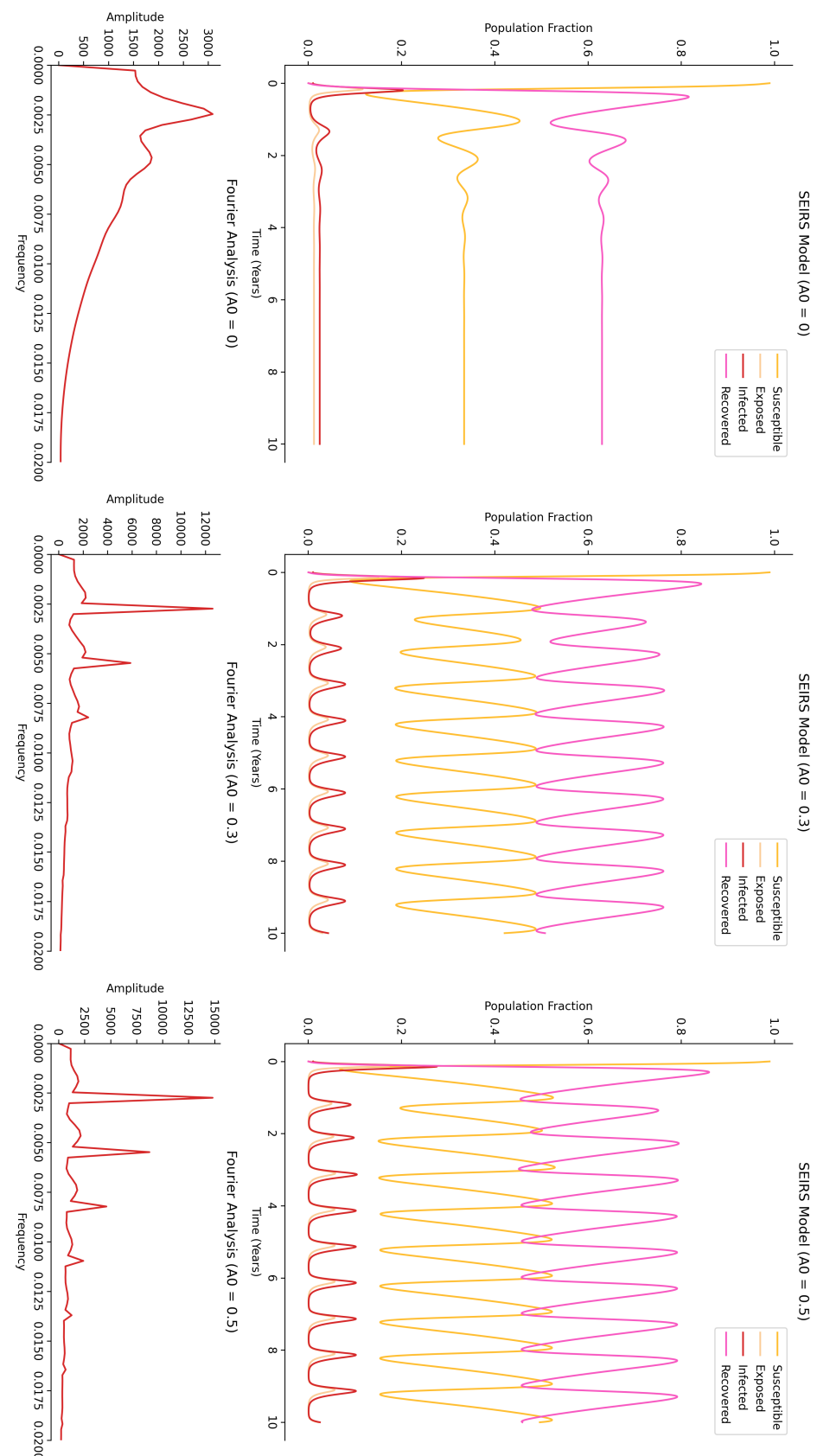


Figure 11: Effect of Seasonal Forcing on SEIRS with Fourier Analyses

## References

- [1] M. A. Spyrou, M. Keller, R. I. Tukhbatova, *et al.*, “Phylogeography of the second plague pandemic revealed through analysis of historical yersinia pestis genomes,” *Nature Communications*, vol. 10, no. 1, p. 4470, Oct. 2019, ISSN: 2041-1723. DOI: 10.1038/s41467-019-12154-0. [Online]. Available: <https://doi.org/10.1038/s41467-019-12154-0>.
- [2] B. V. Schmid, U. Büntgen, W. R. Easterday, *et al.*, “Climate-driven introduction of the black death and successive plague reintroductions into europe,” en, *Proc. Natl. Acad. Sci. U. S. A.*, vol. 112, no. 10, pp. 3020–3025, Mar. 2015.
- [3] W. O. Kermack and A. G. McKendrick, “A Contribution to the Mathematical Theory of Epidemics,” *Proceedings of the Royal Society of London. Series A, Containing Papers of a Mathematical and Physical Character*, vol. 115, no. 772, pp. 700–721, 1927, Publisher: The Royal Society, ISSN: 09501207. [Online]. Available: <http://www.jstor.org/stable/94815> (visited on 09/25/2023).
- [4] M. J. Keeling and P. Rohani, *Modeling Infectious Diseases in Humans and Animals*, English. Princeton University Press, 2008, ISBN: 978-0-691-11617-4.
- [5] A. Best, *Introducing Mathematical Biology*, 1st. University of Sheffield Pressbooks, 2023.
- [6] S. H. Strogatz, *Nonlinear Dynamics and Chaos: With Applications to Physics, Biology, Chemistry, and Engineering*, 2nd. Westview Press, 2014.
- [7] O. N. Bjørnstad, K. Shea, M. Krzywinski, and N. Altman, “The seirs model for infectious disease dynamics,” *Nature Methods*, vol. 17, no. 6, pp. 557–558, Jun. 2020, ISSN: 1548-7105. DOI: 10.1038/s41592-020-0856-2. [Online]. Available: <https://doi.org/10.1038/s41592-020-0856-2>.
- [8] T. Heikkinen and A. Järvinen, “The common cold,” *The Lancet*, vol. 361, no. 9351, pp. 51–59, Jan. 2003, ISSN: 0140-6736. DOI: 10.1016/S0140-6736(03)12162-9. [Online]. Available: [https://doi.org/10.1016/S0140-6736\(03\)12162-9](https://doi.org/10.1016/S0140-6736(03)12162-9).
- [9] M. M. Patel, I. A. York, A. S. Monto, M. G. Thompson, and A. M. Fry, “Immune-mediated attenuation of influenza illness after infection: Opportunities and challenges,” *The Lancet Microbe*, vol. 2, no. 12, e715–e725, Dec. 2021, ISSN: 2666-5247. DOI: 10.1016/S2666-5247(21)00180-4. [Online]. Available: [https://doi.org/10.1016/S2666-5247\(21\)00180-4](https://doi.org/10.1016/S2666-5247(21)00180-4).
- [10] A. C. Lowen and J. Steel, “Roles of humidity and temperature in shaping influenza seasonality,” en, *J. Virol.*, vol. 88, no. 14, pp. 7692–7695, Jul. 2014.
- [11] C. R. Harris, K. J. Millman, S. J. van der Walt, *et al.*, “Array programming with NumPy,” *Nature*, vol. 585, no. 7825, pp. 357–362, Sep. 2020. DOI: 10.1038/s41586-020-2649-2. [Online]. Available: <https://doi.org/10.1038/s41586-020-2649-2>.
- [12] P. Virtanen, R. Gommers, T. E. Oliphant, *et al.*, “SciPy 1.0: Fundamental Algorithms for Scientific Computing in Python,” *Nature Methods*, vol. 17, pp. 261–272, 2020. DOI: 10.1038/s41592-019-0686-2.
- [13] J. D. Hunter, “Matplotlib: A 2d graphics environment,” *Computing in Science & Engineering*, vol. 9, no. 3, pp. 90–95, 2007. DOI: 10.1109/MCSE.2007.55.
- [14] W. H. Press, S. A. Teukolsky, W. T. Vetterling, and B. P. Flannery, *Numerical Recipes 3rd Edition: The Art of Scientific Computing*, 3rd ed. Cambridge University Press, 2007, ISBN: 0521880688. [Online]. Available: [http://www.amazon.com/Numerical-Recipes-3rd-Scientific-Computing/dp/0521880688/ref=sr\\_1\\_1?ie=UTF8&s=books&qid=1280322496&sr=8-1](http://www.amazon.com/Numerical-Recipes-3rd-Scientific-Computing/dp/0521880688/ref=sr_1_1?ie=UTF8&s=books&qid=1280322496&sr=8-1).
- [15] I. Goodfellow, Y. Bengio, and A. Courville, *Deep Learning*. MIT Press, 2016, <http://www.deeplearningbook.org>.